

A lower limb exoskeleton control system based on steady state visual evoked potentials

This content has been downloaded from IOPscience. Please scroll down to see the full text.

2015 J. Neural Eng. 12 056009

(<http://iopscience.iop.org/1741-2552/12/5/056009>)

View the [table of contents for this issue](#), or go to the [journal homepage](#) for more

Download details:

IP Address: 181.170.194.93

This content was downloaded on 12/02/2016 at 03:12

Please note that [terms and conditions apply](#).

A lower limb exoskeleton control system based on steady state visual evoked potentials

No-Sang Kwak¹, Klaus-Robert Müller^{1,2} and Seong-Whan Lee^{1,3}

¹ Department of Brain and Cognitive Engineering, Korea University, Anam-dong, Seongbuk-ku, Seoul, Korea

² Machine Learning Group, Department of Computer Science, TU Berlin, Berlin, Germany

E-mail: nskwak@korea.ac.kr, klaus-robert.mueller@tu-berlin.de and sw.lee@korea.ac.kr

Received 1 April 2015, revised 1 July 2015

Accepted for publication 3 July 2015

Published 17 August 2015



Abstract

Objective. We have developed an asynchronous brain–machine interface (BMI)-based lower limb exoskeleton control system based on steady-state visual evoked potentials (SSVEPs). *Approach.* By decoding electroencephalography signals in real-time, users are able to walk forward, turn right, turn left, sit, and stand while wearing the exoskeleton. SSVEP stimulation is implemented with a visual stimulation unit, consisting of five light emitting diodes fixed to the exoskeleton. A canonical correlation analysis (CCA) method for the extraction of frequency information associated with the SSVEP was used in combination with k -nearest neighbors. *Main results.* Overall, 11 healthy subjects participated in the experiment to evaluate performance. To achieve the best classification, CCA was first calibrated in an offline experiment. In the subsequent online experiment, our results exhibit accuracies of $91.3 \pm 5.73\%$, a response time of 3.28 ± 1.82 s, an information transfer rate of 32.9 ± 9.13 bits/min, and a completion time of 1100 ± 154.92 s for the experimental parcour studied. *Significance.* The ability to achieve such high quality BMI control indicates that an SSVEP-based lower limb exoskeleton for gait assistance is becoming feasible.

Keywords: brain–machine interface, electroencephalogram, steady state visual evoked potentials, exoskeleton control

(Some figures may appear in colour only in the online journal)

1. Introduction

Brain–machine interfaces (BMIs) are communication systems in which the user’s intention is conveyed to the external world through devices without involving the normal output pathways of peripheral nerves and muscles [1, 2]. Invasive and non-invasive BMIs have raised hope for patients suffering from motor disabilities (e.g., [3, 4]). Several research groups have developed BMI techniques, which allow users to control external devices such as wheelchairs (e.g., [5, 6]) or robot arms (e.g., [7, 8]).

One of the most popular neurophysiological signatures used in BMI research is the modulation of sensorimotor

rhythms through motor imagery (MI) [9]. Imagination of limb movement (e.g. right/left hand or foot movement) produces distinctive lateralized patterns on the motor cortex that can be detected. Of similar importance are BMIs that are based on event related potentials (ERP), e.g. the highly popular P300 spellers based on visual or auditory paradigms (cf [10, 11]). Recently, efficient feature extraction and classification methods of MI and ERP have been introduced (cf [12–18]).

However, MI-based systems are limited by the comparatively low number of reliable control commands that can be decoded. In addition, there are a considerable number of users that are unable to control a MI-based BMI [19]. Also, in general, BMI studies are typically performed while the subjects are sitting. Any subject mobility creates challenging

³ Author to whom any correspondence should be addressed.

motion artifacts in the EEG signal (see [20]); moreover it is difficult for subjects to engage in MI while moving.

In the following, we will use an SSVEP based BMI since it can provide a relatively high signal-to-noise ratio (SNR) and information transfer rate (ITR) (e.g. [10, 21]). Each SSVEP command is associated with repetitive visual stimuli that have a distinctive frequency. The user's attention can selectively focus on the visual stimulus, then an oscillatory SSVEP component manifests itself in the subject's visual cortex that matches the frequency (and higher harmonics) of the attended stimulus. SSVEPs can be elicited by repetitive visual stimuli at frequencies in the 1 to 100 Hz range [23]. This frequency locking can be decoded in various manners; e.g. common spatial patterns (CSP) [12] can classify SSVEP with low error without time delay. However, long training times may be needed to achieve high accuracy [24]. Stimulus-locked inter-trace correlation (SLIC) is suitable for irregular stimulus patterns [25]. The least absolute shrinkage and selection operator (LASSO)-based SSVEP classifiers typically yield higher ITR than other methods [26]. The CCA method for multi channel SSVEP detection shows increased detection accuracy, since it can also recognize and harvest from harmonic frequencies [27].

Other research has shown the feasibility of electrical hand prosthesis control with SSVEPs for healthy subjects in which flickering lights were mounted on the surface of the neuroprosthesis [21], and patients with tetraplegia [22]. An orthosis could lift up a leg whilst sitting and was controlled using SSVEP [28]. Asynchronous BCI control using a high-frequency SSVEP was introduced [29]. Also, visual evoked responses (P300) [20] and SSVEP [30] were detected during walking. Brain activity accompanying cognitive processes during whole body movement while driving [31] or in working environments [32] was analysed.

Recent studies have proved the possibility of decoding the user's walking intentions within a virtual reality environment [33], or using an exoskeleton [34–36]. Also applications of BMI systems in stroke recovery and rehabilitation (see [37]) and hybrid assertive limb systems [38, 39] have been developed. In addition, a recent study investigated the use of an fNIRS-BCI to detect the preparation for the movement of the hip in subjects who have suffered a stroke [40]. Other research showed that EEG has valuable information for the decoding of expressive human movement [41]. Although BMI systems have shown great success in many studies, a future translation of closed-loop neuroprosthetic devices from the laboratory to the market still requires better long-term device reliability, robustness and safety [42]. Furthermore, significant challenges still exist for the development of a lower limb exoskeleton that can integrate with the user's neuromusculoskeletal system [43].

In our study on healthy subjects, we will use non-invasive EEG-based systems for controlling an exoskeleton. Here, EEG is advantageous due to its reliability, safety, ease of acquisition, and cost effectiveness compared with other modalities; furthermore the SSVEP paradigm shows remarkable robustness with respect to artifacts that originate from the exoskeleton and walking movements.

In our preliminary study [44], we reported on an elementary prototype of an SSVEP controlled exoskeleton for a few subjects in an offline experiment design. In this work, we provide a more elegant method for the online control of the exoskeleton despite its excessive EEG artifacts. In addition, offline and online experiments, experimental results, performance evaluations and extensive analysis are given.

In this paper, we therefore demonstrate that a lower limb exoskeleton control system can be successfully operated asynchronously using an SSVEP-based BMI. Exoskeletons can create severe artifacts that make free EEG recordings unfeasible. Only by virtue of the oscillatory nature of SSVEP can we decode user intention *despite* the highly unfavourable signal to noise ratio, as nicely shown in our offline evaluation. Also, an asynchronous BMI system is difficult to implement due to rest or idle states when the user does not look at any flickering light. Hence, we implement a robust asynchronous BMI system including an adjustable threshold to detect and compensate for rest or idle state activities. In addition, an SSVEP-based BMI online control of an exoskeleton as a gait assistant robot is demonstrated.

2. Materials and methods

2.1. Subjects

Eleven healthy subjects, with normal or corrected to normal vision and no history of neurological disease participated in this study (age range, 25–32 years old; 11 males). All experiments were conducted according to the principles expressed in the Declaration of Helsinki. This study was reviewed and approved by the Institutional Review Board at Korea University [1040548-KU-IRB-14-166-A-2] and written informed consent was obtained from all participants before the experiments.

2.2. Components of the system

The SSVEP based exoskeleton control system consists of (i) a signal processing and (ii) a device control part (figure 1(a)). In (i) a PC receives EEG data from a wireless EEG interface (MOVE system, Brain Products GmbH, 8 Ag/AgCl electrodes [PO7, PO3, PO, PO4, PO8, O1, Oz, and O2]) in figure 2, analyses the frequency information, and then provides (ii) the control command to the robotic exoskeleton (Rex, Rex Bionics Ltd.). A visual stimulation unit which was controlled by a micro controller unit (Atmega128) presented visual stimuli using five LEDs. The EEG reference electrode is mounted on the FCz and the ground electrode on Fpz. All impedances were maintained below 10 k Ω ; the sampling frequency rate was 1 kHz. The acquired EEG data was transmitted using a 2 s sliding window size with a 0.5 s shift. A 60-Hz notch filter was applied to the EEG data for removing AC power supply noise.

2.2.1. Exoskeleton. The advantages of the exoskeleton used in this study are that it is self balancing, self supporting and has programmed motions (e.g. walking, turning, sitting,

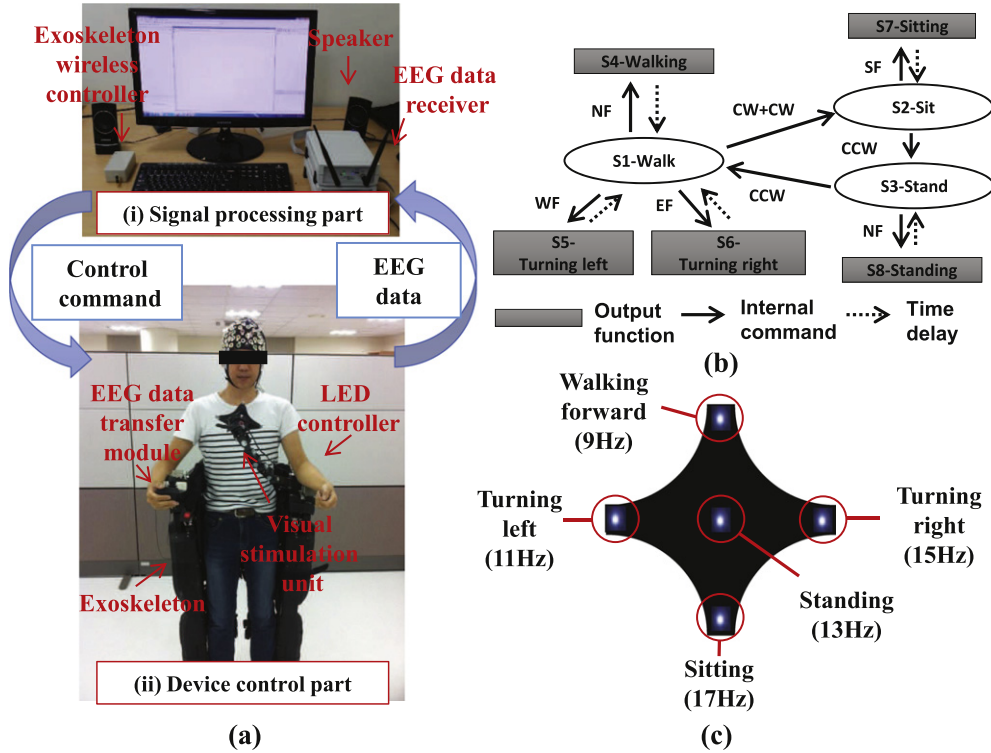


Figure 1. (a) Components of an SSVEP-based exoskeleton system. (b) State machine diagram. (c) Visual stimulation unit.

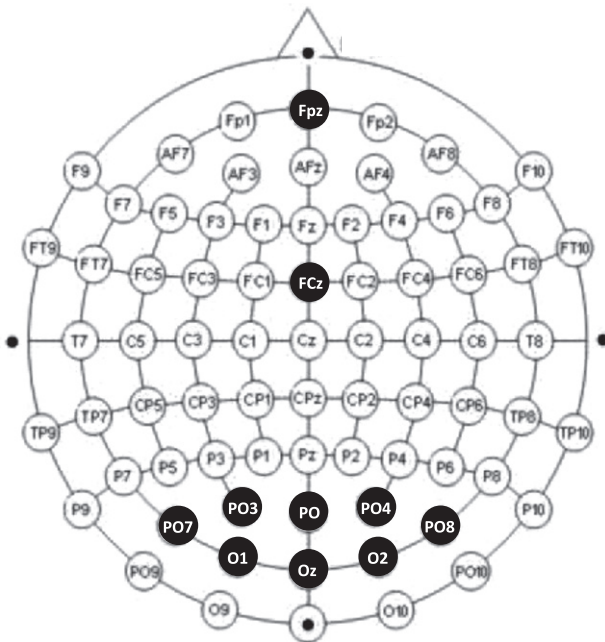


Figure 2. Ground (Fpz), reference (FCz) and eight electrode layout in 10–20 system.

standing and shuffling). It thus enables a person to move by joystick control or by wireless interface. The walking speed and the angle of turning degree of the exoskeleton are approximately 0.1 ms^{-1} and 30° respectively. The Rex wireless interface (FTDI FT232R USB serial interface) consists of paired units: a sender unit connected to the PC via a USB cable and a receiver unit mounted in the Rex arm

stand. The serial port baud rate is 115200 bps using an 8-bit format, no parity and one stop bit. All multi-byte data was sent/received using a little-endian (LSB first). The only functionality provided by the wireless interface is the remote control of the Rex joystick operation (i.e. North Full (NF), South Full (SF), West Full (WF), East Full (EF), Clock Wise (CW) and Counter Clock Wise (CCW)). We have designed a state machine diagram to intuitively describe the system's behavior (figure 1(b)).

2.2.2. Visual stimulation unit. The visual stimulation unit is made out of an arm stand, five LEDs and a micro controller unit. The arm stand (IK-208, Ilkwang Inc.), with a weight of 1.3 kg and a length of 65 cm, is freely deformable. On the head of the arm stand, four squared-shaped multi-chip high flux LEDs (DG-82A83C-001-5/S-3), with a luminous intensity of 6000 mcd, a peak wavelength of 0.26/0.28 nm and a white emitting color, were attached. Figure 1(c) shows the locations of each LED. Their continuous flickering allows a command for walking forward, turning left, standing, turning right, and sitting. Previous research showed a higher amplitude of SSVEPs in the frequency range of 10 to 15 Hz than for other frequency bands [45]. Hence, we selected frequencies of LEDs with a 2 Hz interval to minimize the influence of adjacent stimuli. Consequently, LEDs are operated in 9, 11, 13, 15, and 17 Hz respectively and with a 0.5 duty ratio.

2.3. Signal processing

Canonical correlation analysis (CCA) is used for decomposing the EEG signal in order to extract stimulation frequency

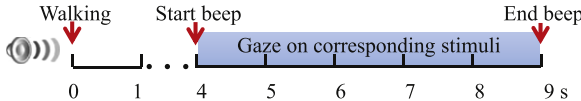


Figure 3. An example of the offline experimental paradigm.

related information. CCA (see [27, 46, 47]) is a multivariable statistical method that finds a pair of linear combinations such that the correlation between two canonical variables X and Y is maximized. As one data set, $X(t)$, we choose 2 s windows of EEG; as $Y_i(t)$ we use the five reference frequencies ($f_1 = 9$, $f_2 = 11, \dots, f_5 = 17$) from the five visual stimuli

$$Y_i(t) = (\sin(2\pi f_i t), \cos(2\pi f_i t), \sin(2\pi(2f_i)t), \cos(2\pi(2f_i)t))', t = \frac{1}{S}, \frac{2}{S}, \dots, \frac{T}{S} \quad (1)$$

T is the number of sampling points, and S denotes the sampling rate.

CCA finds the weight vectors, W_x and W_y , which maximize the correlation between the canonical variants $x = X^T W_x$ and $y = Y^T W_y$, by solving

$$\begin{aligned} \max_{W_x, W_y} \rho(x, y) &= \frac{E[x^T y]}{\sqrt{E[x^T x] E[y^T y]}} \\ &= \frac{E[W_x^T X Y^T W_y]}{\sqrt{E[W_x^T X X^T W_x] E[W_y^T Y Y^T W_y]}}. \end{aligned} \quad (2)$$

The maximum of ρ with respect to W_x and W_y is the maximum canonical correlation. The canonical correlation ρ is used for detecting the respective frequency of the LED that the subject attended.

We use simple thresholding to increase the robustness for controlling in an asynchronous mode. The thresholds of ρ_i for five frequencies are determined by $Tr_i = \text{mean}(\rho_i) - \text{SD}(\rho_i)$, where $\rho_i (i = 1, 2, \dots, 5)$ is a set of the maximized correlation of correctly classified trials. The control commands used in the online experiment are transmitted when two conditions are satisfied: (i) the correlation values between the EEG and the five reference data need to exceed a threshold value, and (ii) this value is the highest one compared with the correlation values for the potential alternative classes.

2.4. Offline experiment

The main purpose of this offline experiment is to find the threshold values of the canonical correlation for asynchronous online control. The subjects were instructed to attend in random order to the specific LED indicated to them by an auditory cue while standing inside the exoskeleton (see figure 3). All LEDs were simultaneously blinking during the offline experiment. After the random auditory cue, a start beep sound follows 3 s later, then the subjects look at the corresponding LED for 5 s. Each command was presented 10 times (50 trials in total).

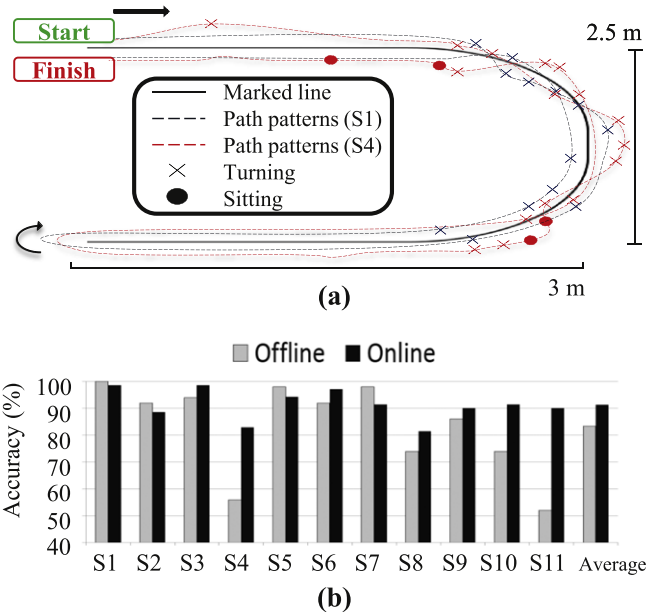


Figure 4. (a) Experimental environment of task two and path patterns of two subjects. (b) Comparison of offline accuracy (gray) with online accuracy (black).

2.5. Online experiments

To assess the online BMI performance we designed two tasks. First, we measured the accuracy and response time of SSVEP detection to study the time needed to focus on the flickering LEDs. We also calculated the information transfer rate (ITR). Second, we measured the completion time needed to finish the whole walking course which we had designed.

2.5.1. Task 1. The subjects are asked to visually attend to LEDs given by auditory cues while standing in the exoskeleton. The next cue is always given after observing the subject's response; trials with no response during 10 seconds are regarded as a failure. In this task, each class/command has 15 trials (70 trials in total).

2.5.2. Task 2. The subjects perform a sit/stand task 10 times each and then follow a line marked on the ground in a clockwise direction until a finish line and return counter clockwise—in total approximately 17 m. We mandatorily rotated the exoskeleton when subjects reached the 180° turning point due to limitations in the mechanical functions of the exoskeleton (see figure 4(a) and video at: www.youtube.com/watch?v=y8aeX6AXzlc).

2.6. Evaluation of classifier

We evaluated the performance of three classifiers by assessing the maximum value of CCA, by a threshold of CCA, and by a k -nearest neighbors (KNN) algorithm using offline and online experiment data. For KNN, the set of canonical correlations (ρ_i) is used as a feature for classification.

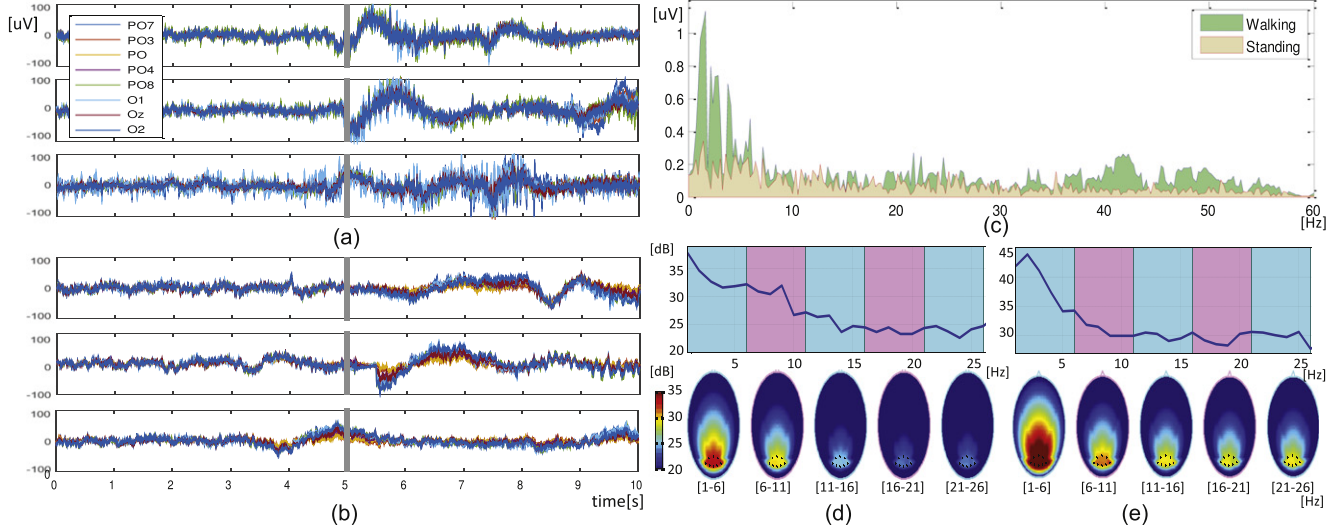


Figure 5. (a) Examples of EEG data of S8 during standing and walking with an exoskeleton. (b) Examples of EEG data of S1. The gray line indicates starting time to walk. (c) Comparison of FFT results of (a); artifacts are in all frequency bands. In particular, a high amount of artifacts are induced in the low band. (d) Power spectra of EEG data during standing and topography maps at five frequency bands from 1 to 26 with a 5 Hz interval. (e) Power spectra during walking and topography maps at five frequency bands from 1 to 26 with a 5 Hz interval.

Table 1. Mean, SD, and kurtosis of offline data.

Offline		S1	S2	S3	S4	S5	S6	S7	S8	S9	S10	S11	Average
1–6 Hz	mean	0.03	-0.07	0.05	0.03	0.07	-0.03	-0.01	-0.01	-0.17	-0.40	-0.15	-0.06
	SD(\pm)	1.04	2.00	0.83	0.35	0.55	0.50	0.53	0.53	0.99	2.85	0.64	0.98
	kurtosis	2.78	2.55	2.50	3.18	2.64	3.02	1.95	1.95	2.47	4.65	2.28	2.72
6–11 Hz	mean	-0.02	-0.01	-0.01	0.00	0.00	-0.01	0.00	0.00	-0.01	0.01	-0.01	0.00
	SD(\pm)	0.36	1.00	0.33	0.27	0.38	0.27	0.25	0.25	0.28	1.22	0.34	0.45
	kurtosis	3.19	5.29	2.65	2.93	2.44	2.94	2.55	2.55	2.76	6.04	3.42	3.34
11–16 Hz	mean	0.00	0.00	0.01	-0.01	0.00	0.00	0.00	0.00	-0.01	0.00	0.00	0.00
	SD(\pm)	0.25	0.44	0.31	0.22	0.26	0.23	0.24	0.24	0.38	0.87	0.43	0.35
	kurtosis	3.51	3.34	3.43	3.73	3.16	3.11	3.99	3.99	1.85	4.19	3.53	3.44
16–21 Hz	mean	0.00	0.00	0.00	0.00	0.00	0.00	0.00	0.00	0.01	0.00	0.00	0.00
	SD(\pm)	0.27	0.26	0.30	0.21	0.39	0.28	0.20	0.20	0.42	0.50	0.29	0.30
	kurtosis	2.48	2.94	3.65	3.20	3.68	3.02	3.48	3.48	3.49	4.22	2.71	3.30
21–26 Hz	mean	0.00	0.01	0.00	0.00	0.00	0.00	0.00	0.00	0.01	0.00	0.00	0.00
	SD(\pm)	0.32	0.26	0.25	0.23	0.27	0.34	0.18	0.18	0.78	0.66	0.26	0.34
	kurtosis	3.09	3.42	3.78	2.39	4.13	2.87	2.67	2.67	3.29	2.80	3.60	3.15
26–31 Hz	mean	0.00	0.00	0.00	0.00	0.00	0.00	0.00	0.00	0.00	0.00	0.00	0.00
	SD(\pm)	0.19	0.12	0.16	0.21	0.15	0.27	0.14	0.14	0.47	0.38	0.19	0.22
	kurtosis	3.53	2.95	2.80	2.77	3.42	2.43	3.64	3.64	4.56	6.02	2.45	3.47
31–36 Hz	mean	0.00	0.00	0.00	0.00	0.00	0.00	0.00	0.00	0.00	0.00	0.00	0.00
	SD(\pm)	0.14	0.19	0.17	0.17	0.17	0.19	0.12	0.12	0.30	0.33	0.18	0.19
	kurtosis	2.97	2.65	2.71	3.18	4.22	2.88	2.40	2.40	2.73	2.98	3.13	2.93
36–41 Hz	mean	0.00	0.00	0.00	0.00	0.00	0.00	0.00	0.00	0.00	0.00	0.00	0.00
	SD(\pm)	0.11	0.14	0.24	0.11	0.16	0.09	0.10	0.10	0.18	0.35	0.12	0.15
	kurtosis	2.28	3.12	2.13	2.04	3.24	2.96	3.60	3.60	3.08	3.05	2.86	2.91
all freq.	mean	0.30	-0.23	-0.17	-0.30	0.04	-0.04	0.22	0.22	0.16	1.09	0.78	0.19
	SD(\pm)	1.95	2.68	1.52	1.05	1.19	1.07	1.09	1.09	1.92	4.75	1.41	1.79
	kurtosis	2.66	7.12	2.47	3.36	2.81	3.01	3.12	3.12	2.80	6.76	2.27	3.59

3. Results and discussion

When measuring EEG signals as the exoskeleton walks, the exoskeleton can yield different artifacts caused by moving, head swing, or motor sound, etc. Note that even the motor sound can be a source of artifacts. It has been shown that such

an auditory stimulus induces a reliable response (i.e. a significant increase in EEG power at the stimulation frequency [48, 49]). Figure 5(a) shows typical examples of suboptimal trials from S8 in standing and walking conditions while gazing at the 9 Hz stimulus—high artifactual oscillations are induced. EEG data which acquired form S1 under the same

Table 2. Mean, SD, and kurtosis of online data.

Onine		S1	S2	S3	S4	S5	S6	S7	S8	S9	S10	S11	Average
1–6 Hz	mean	0.14	0.01	0.16	-3.57	0.14	0.04	0.15	-0.06	0.00	0.65	-0.11	-0.22
	SD(±)	1.63	1.70	1.83	25.99	1.77	1.33	1.95	2.15	2.04	4.97	5.56	4.63
	kurtosis	2.37	1.84	2.11	2.92	2.97	2.33	2.34	2.65	2.35	3.19	2.21	2.48
6–11 Hz	mean	0.00	-0.02	0.00	0.10	-0.01	0.00	-0.01	-0.02	-0.02	0.01	0.01	0.00
	SD(±)	0.83	0.75	0.82	16.09	0.78	0.35	1.39	1.88	0.89	1.17	4.31	2.66
	kurtosis	3.05	2.34	3.93	2.71	3.49	2.53	2.10	2.85	2.24	2.23	2.48	2.72
11–16 Hz	mean	-0.01	0.00	0.00	0.01	0.00	0.00	0.00	0.01	0.00	0.00	0.00	0.00
	SD(±)	0.46	0.42	0.46	9.54	0.27	0.34	0.62	1.41	0.50	1.06	2.31	1.58
	kurtosis	3.29	2.19	2.69	2.22	2.27	2.84	2.32	3.45	2.59	3.66	3.23	2.80
16–21 Hz	mean	0.00	-0.01	0.01	0.00	0.00	0.00	0.00	0.01	0.00	0.00	0.01	0.00
	SD(±)	0.69	0.35	0.47	6.55	0.24	0.35	0.56	1.33	0.57	1.00	1.70	1.26
	kurtosis	3.49	5.15	1.80	2.81	2.09	2.29	2.62	2.24	2.47	2.44	2.72	2.74
21–26 Hz	mean	0.00	0.01	0.00	0.09	0.00	0.00	0.00	-0.01	0.00	0.01	-0.01	0.01
	SD(±)	0.99	0.43	0.39	5.18	0.37	0.54	0.31	1.42	0.65	1.04	1.37	1.15
	kurtosis	3.70	2.16	3.28	3.37	1.86	2.53	2.78	3.28	3.13	2.54	2.81	2.86
26–31 Hz	mean	0.00	0.00	0.00	-0.06	0.00	0.00	0.00	0.00	0.00	0.00	-0.01	-0.01
	SD(±)	0.35	0.47	0.46	4.30	0.28	0.39	0.33	0.86	0.42	0.81	1.01	0.88
	kurtosis	3.27	3.45	3.02	3.05	2.86	3.99	2.22	3.98	3.46	2.19	2.67	3.11
31–36 Hz	mean	0.00	0.00	0.00	0.02	0.00	0.00	0.00	0.00	0.00	0.00	0.00	0.00
	SD(±)	0.45	0.41	0.31	3.14	0.18	0.41	0.26	0.62	0.34	0.61	1.05	0.71
	kurtosis	2.31	3.94	2.15	2.54	3.09	2.12	2.68	2.98	2.55	2.32	3.59	2.75
36–41 Hz	mean	0.00	0.00	0.00	-0.03	0.00	0.00	0.00	0.00	0.00	-0.01	-0.01	0.00
	SD(±)	0.41	0.37	0.33	3.40	0.21	0.17	0.17	0.70	0.25	0.86	1.26	0.74
	kurtosis	2.28	2.97	2.93	2.44	2.65	3.01	2.67	3.28	2.39	3.43	3.08	2.83
all freq.	mean	-0.16	-0.13	0.20	-6.73	-0.32	0.02	-0.06	-0.49	0.36	1.08	0.16	-0.55
	SD(±)	2.61	3.15	3.13	3.97	2.23	1.97	2.80	5.20	2.96	7.73	8.91	4.06
	kurtosis	2.30	2.71	3.08	3.26	2.60	3.00	2.80	4.08	3.03	2.72	3.33	2.99

conditions is presented in (b). Figure 5(c) shows the FFT results of S8 in the two states. The walking state shows higher amplitudes in all frequency bands. In particular, a large amount of artifacts appear in the low frequency range. Figures 5(d) and (e) show the power spectra and topography maps at five frequency intervals from 1 to 26 Hz. The walking state clearly has larger power and wideband artifacts when compared to the standing state.

More detailed analysis of artifacts are presented in tables 1, 2, and figure 6. In figure 6(a), the mean, SD, and kurtosis are provided for each subject, the average of all subjects, and the average of subjects where the low performance group is excluded (S4, S8, S10, and S11). Figures 6(b) and (c) show an overview of several sub frequency bands for all subjects and subjects excluding the low performance group respectively. The SD of all subjects was affected in walking state compared to standing state. However, the variation of SD is different among subjects. Above all, the subjects who have a large SD (i.e. S4, S8, S10, and S11) showed lower performance than other subjects. Our online experiments were conducted immediately after the training data collection procedure (approximately 8 min). Hence, we surmise that larger artifacts may happen in some subjects and these artifacts may result from the overall experimental setup that is, however, not uncommon in exoskeleton experiments. In particular, the subjects' head movements that occur under ambulatory conditions can give rise to swinging movements in the line

between electrodes and EEG amplifiers. In extreme cases, this may cause a disconnection or high impedance. In particular, subject S4 shows a negative mean value which exemplifies the poor quality of EEG signals and high impedances respectively due to suboptimal EEG recording conditions.

3.1. Offline experiment

The thresholds of ρ_i for the five frequencies are calculated after a short calibration; they vary across subjects. According to the offline accuracy, the subjects who showed good performance (i.e. S1, S5, and S7) generally have higher threshold values than the lower performing subjects (i.e. S4, S8, S10, and S11) (see figure 7). Note that it is helpful to further adjust them immediately prior to the start of the online experiment. Thus, a clear correlation with the first harmonic as well as the second harmonic frequency is observed. Over all subjects we find an average accuracy of 83.27%: six subjects (S1, S2, S3, S5, S6, and S7) show an accuracy 95.67%, whereas two subjects exhibit poor performances at 54% (see figure 4(b)). We surmise that lapses of focused attention on the desired flickering lights during the experiment and/or suboptimal stimulation frequencies may have caused this inability.

3.2. Online experiments

For online control, a misclassification should be avoided as it could potentially lead to dangerous situations for the users

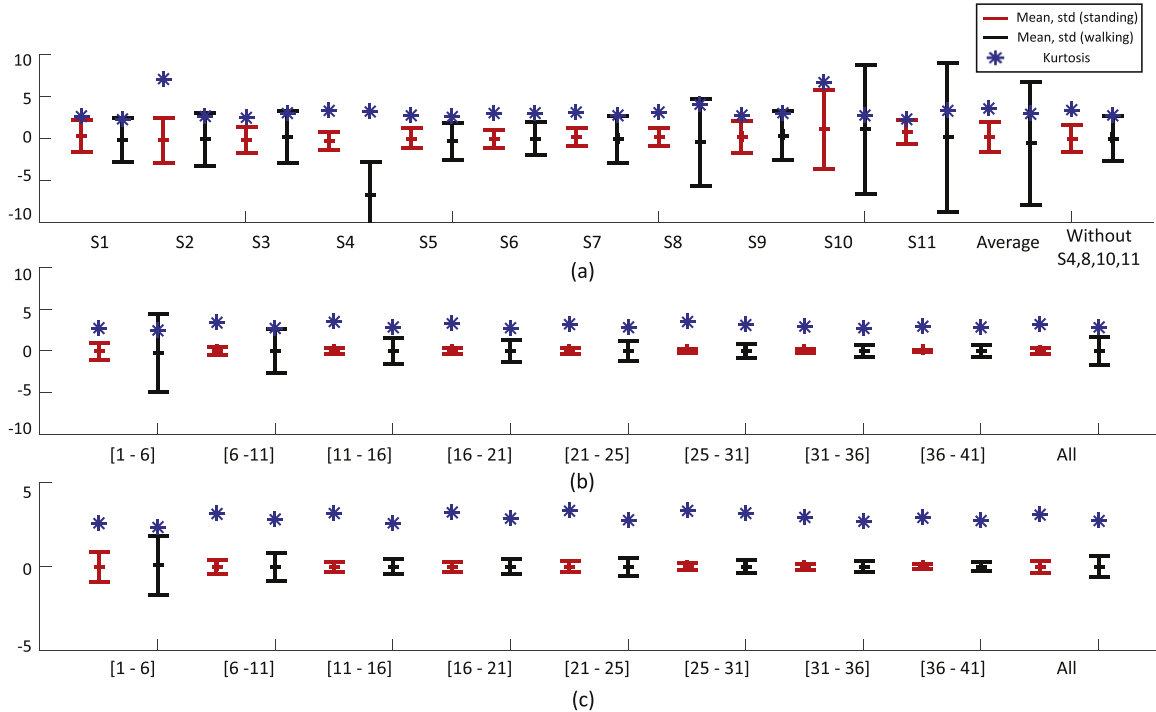


Figure 6. Artifact analysis of standing state (red line) and walking state (black line). Each line indicates mean and SD. Blue asterisk indicates kurtosis. (a) Each subject, the average of all subjects, and subjects excluding the low performance group (S4, S8, S10, and S11). (b) Each sub frequency band for all subjects. (c) Each sub frequency band in subjects excluding the low performance group.

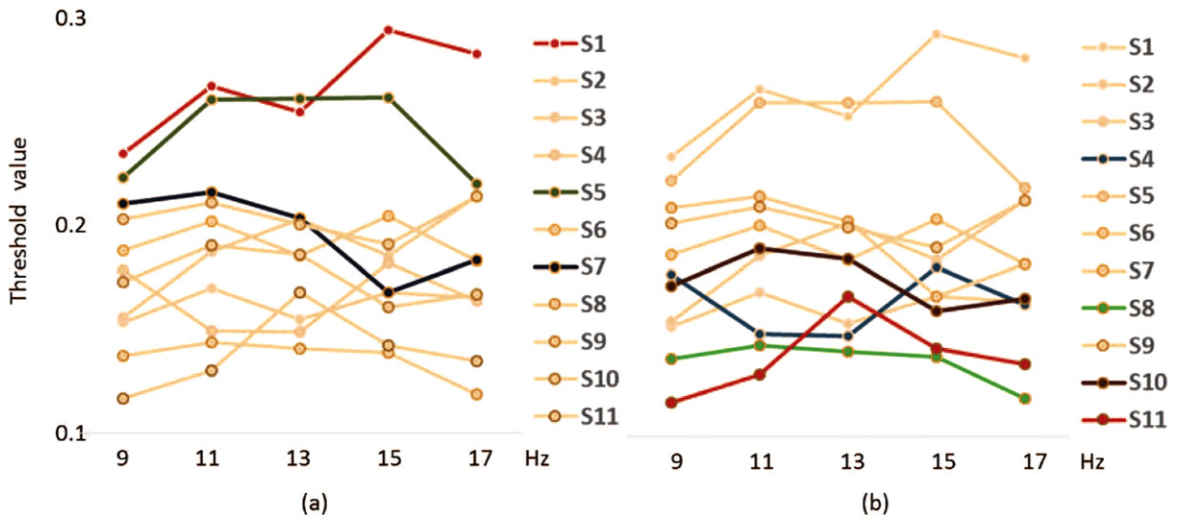


Figure 7. Thresholds for subjects with (a) high and (b) low performance.

controlling the exoskeleton. Also, for asynchronous BMI, idle or rest states should be classified with certainty as rest class; thus thresholds should be set conservatively.

In the offline experiment, the EEG data was classified by finding the maximum of the canonical correlations between all classes. After a short calibration, these threshold values were calculated and were then used for the online experiment. Hence, online accuracy (91.3 %) can even increase by 8.03% when compared to the average of offline accuracy (figure 4(b)). Above all, subject S4 and S11 show a large improvement in accuracy (respectively 26.86% and 38%).

The reasons for the large increases in accuracy for S4 and S11 in the online experiment as compared to the offline experiment are explained in figure 8. We compare the canonical correlation variation with two classification methods: by maximum correlation (figure 8(a)) and the threshold value method (figure 8(b)). For this we analyse data from subject S11 in an exemplary manner. Each color denotes the corresponding class. The vertical and horizontal lines indicate the auditory cue and threshold value respectively. The gray regions are windows which are selected with the highest accuracy throughout all trials. Furthermore, the correlation

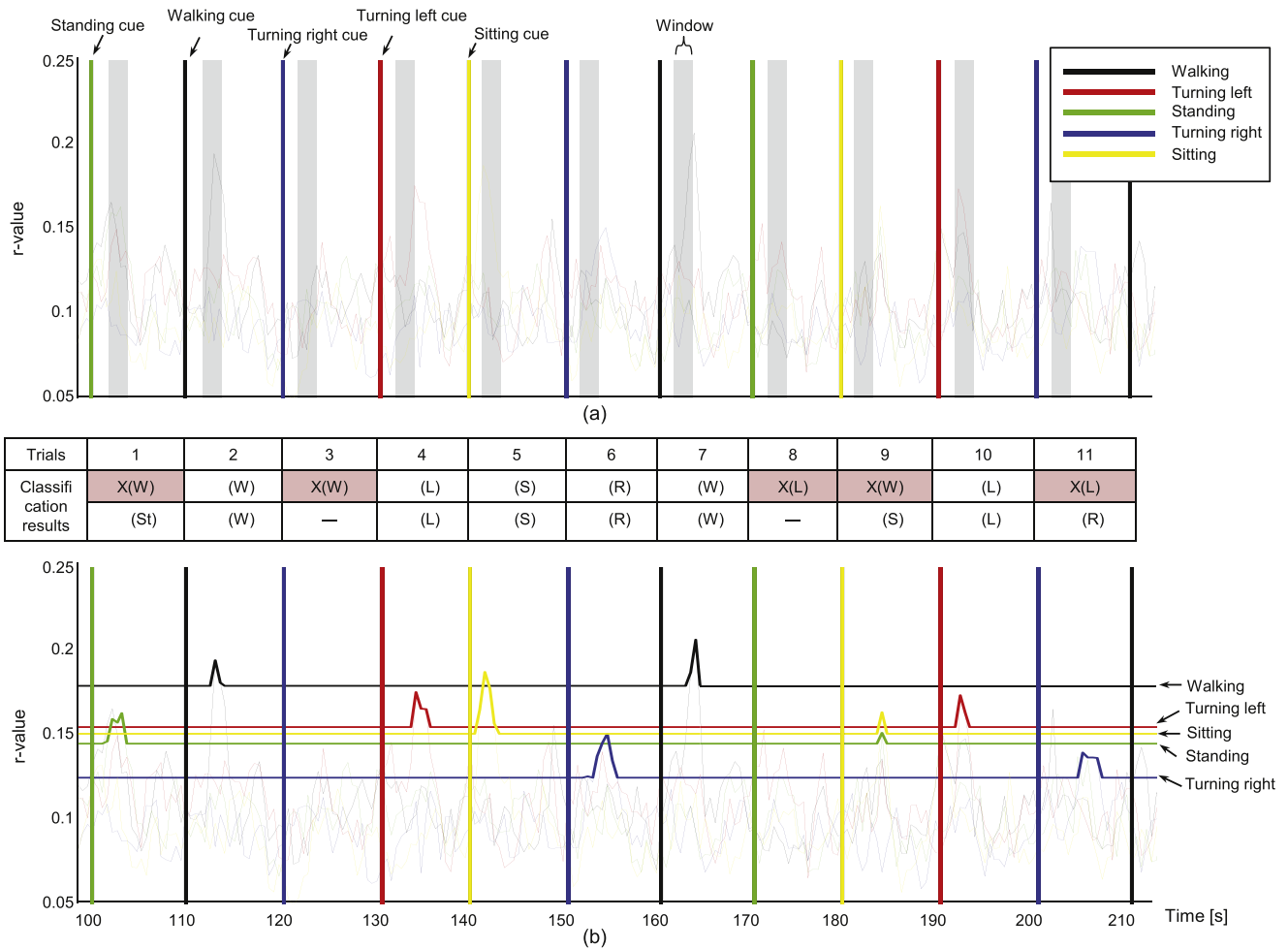


Figure 8. (a) Classification by maximum correlation value. (b) Classification by threshold method for subject S11. Each color means corresponding class. Gray rectangle is a 2 s window. Vertical and horizontal lines are the auditory cue and the threshold value respectively. ‘o’, ‘x’, and ‘—’ indicate correct (true positive—TP), incorrect (false positive—FP), no detection (false negative—FN).

Table 3. Response time and online accuracy of task one. Response time: time spent on focusing until a correct movement was triggered (Mean \pm Std).

Subject	Response time [s]	Accuracy [%]	ITR [bits m ⁻¹]
S1	3.23 \pm 1.01	98.57	40.6
S2	3.34 \pm 2.12	88.57	28.4
S3	2.57 \pm 1.30	98.57	51
S4	3.24 \pm 2.35	82.86	24.4
S5	3.34 \pm 1.57	94.29	34
S6	2.96 \pm 1.28	97.14	42.1
S7	3.1 \pm 1.65	92.86	35
S8	3.86 \pm 2.27	81.43	19.6
S9	3.99 \pm 2.41	90	24.9
S10	3.69 \pm 2.05	91.43	28.1
S11	2.93 \pm 1.48	90	33.8
Average	3.29 \pm 1.83	91.3 \pm 5.73	32.9 \pm 9.13

Table 4. Results of task two. The number of successful sit/stands and the completion time of a line tracing task.

Subject,	successful sit/stand and	completion time [s]
S1	20	942
S2	20	892
S3	20	1132
S4	20	1332
S5	20	1108
S6	18	1406
S7	20	1072
S8	20	1028
S9	18	1119
S10	17	1099
S11	18	970
Average	19.18 \pm 1.17	1100 \pm 154.92
Joystick	—	543

values which are over the corresponding threshold value are plotted as a bold line. For example, in the 1st, 9th and 11th trial, after an auditory cue was given, the data was misclassified by maximum correlation (False Positive, FP).

However, the data was nevertheless classified correctly by the threshold method because only the correct correlation exceeds the threshold (True Positive, TP). The 3rd and 8th trials were also misclassified. However, these trials were regarded as rest

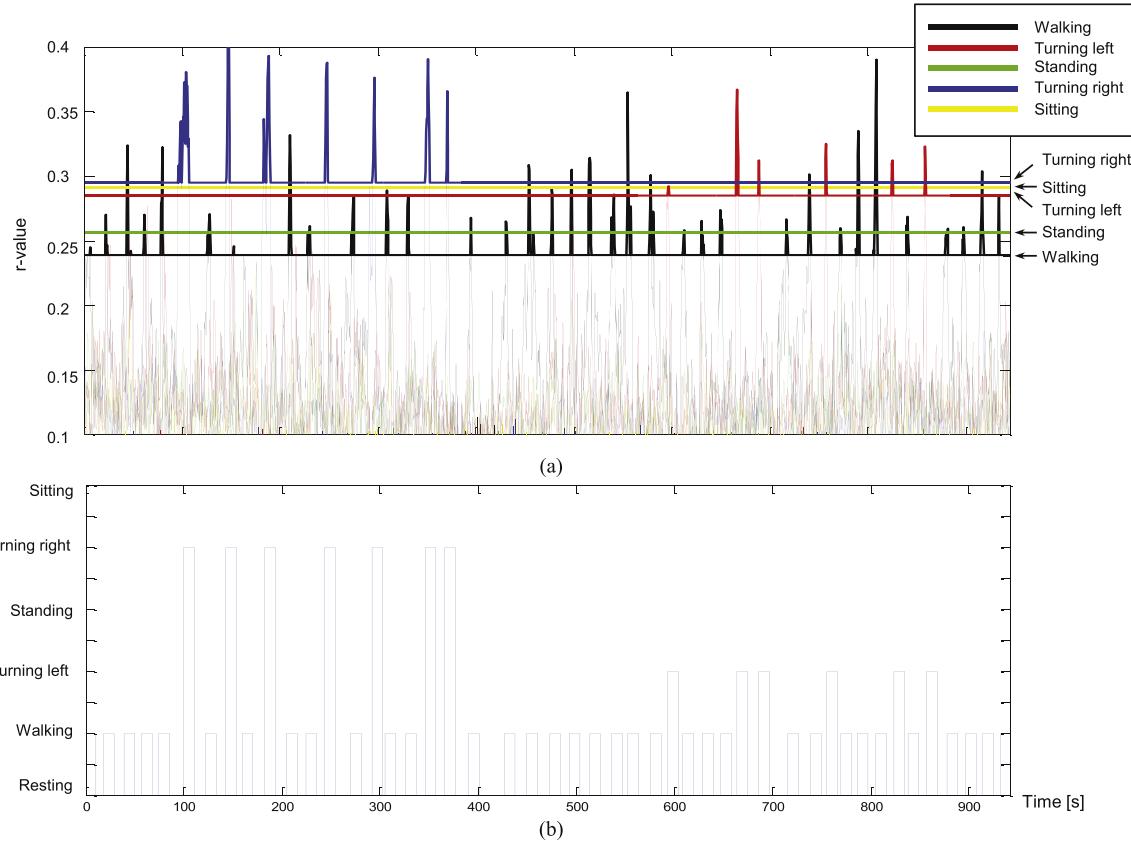


Figure 9. (a) Canonical correlation changes for S1 during line tracing task. Horizontal lines indicate the calculated threshold value from offline experiments. (b) Performed command.

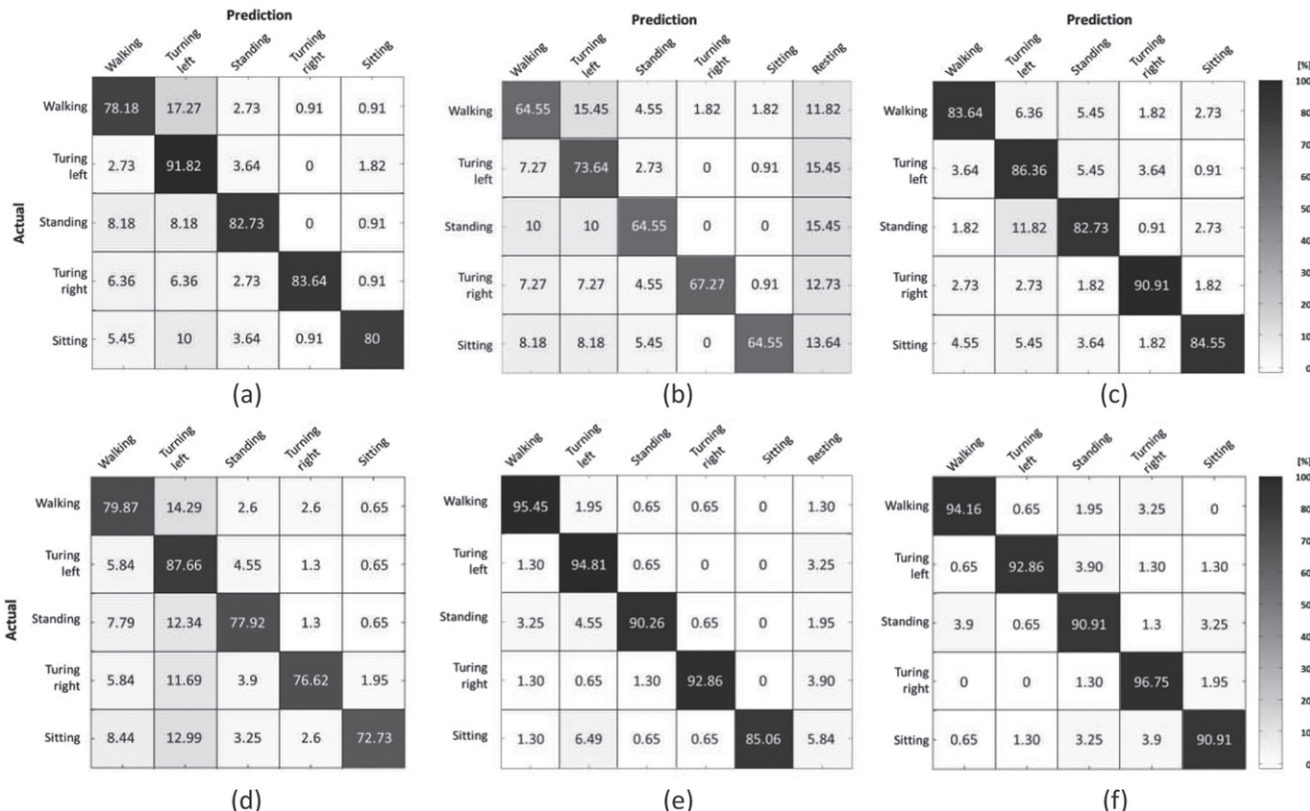


Figure 10. Confusion matrix of offline data classification results by maximum value (a), by threshold (b), and by KNN when $k = 5$ (c). Confusion matrix of online data classification results by maximum value (d), by threshold (e), and by KNN when $k = 5$.

Table 5. The accuracy [%] of offline and online data by threshold using fivefold cross-validation for all subjects.

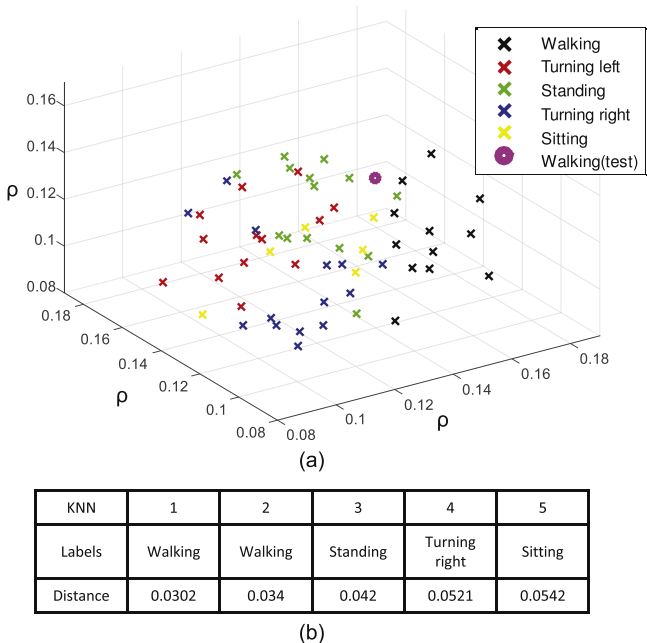
Data \ Subject											
	S1	S2	S3	S4	S5	S6	S7	S8	S9	S10	Average
Offline	82	82	78	54	80	68	68	54	62	62	66.91
Online	95.71	82.85	92.85	88.57	92.85	87.14	95.71	80	92.85	82.85	88.31

Table 6. The accuracy [%] of offline and online data by KNN using fivefold cross-validation for all subjects when k = 5.

Data \ Subject	S1	S2	S3	S4	S5	S6	S7	S8	S9	S10	Average
Offline	98	92	94	52	100	92	100	62	86	76	83.27
Online	100	92.86	98.57	91.43	97.14	94.29	97.14	85.71	97.14	82.86	92.6

Table 7. KNN results of offline and online data using fivefold cross-validation when k = 1, 3, 5, 7 and threshold results using fivefold cross-validation.

Data \ KNN	KNN				Threshold
	1	3	5	7	
Offline	80.18	82	83.27	82.36	66.91
Online	91.04	91.69	92.6	92.07	88.31

**Figure 11.** An example of KNN for S2; test data (purple diamond) with all training data is plotted on the ρ_1 , ρ_2 , and ρ_3 axis (a). The distance of the Kth nearest neighbor and labels when k = 5 of KNN.

class by the threshold method (False Negative, FN). In addition, there were two exceeded correlations (sitting and standing) in the 9th trial, but the classification result was sitting because the threshold for the sitting state was higher than for standing.

The average response time was 3.29 ± 1.83 s which means that the subject needed between 2.57 and 3.99 s to

correctly control the exoskeleton. The information transfer rate (ITR) expressed in bits m^{-1} is the most commonly used criterion to assess the overall performance of BMI [50]:

$$ITR = \left(\frac{60}{T} \right) (p \log_2(p) + (1-p)\log_2\left(\frac{1-p}{N-1}\right) + \log_2(N)) \quad (3)$$

where T is the time needed to convey each command, p is the accuracy, and N is the number of classes (in our study, $N = 5$). The average ITR was 32.9 bits m^{-1} (range: 19.6 to 51 bits m^{-1}).

Note that the individual variation is high: while subject S3 responded with only 2.57 ± 1.3 s and an ITR of 51 bits m^{-1} , subject S8 who exhibited poor classification accuracy during task one also revealed a slow online performance of 3.86 ± 2.27 s and an ITR of 19.6 bits m^{-1} while controlling the exoskeleton (see table 3 for an overview).

The number of successful sit/stand tasks is 19.18 out of 20 times when averaging across subjects. The reason for such high accuracy is that a state machine was designed to recognize only the stand command while the exoskeleton is in the sit position. Note that the system is therefore not a five-class decoder at all times; for example, the exoskeleton does not turn right from a sitting position (see figure 1(b)). Despite the fact that the standing and sitting commands can be designed as toggle switches, the two commands are located separately with different frequencies in the visual stimulation unit.

The average completion time needed to finish the BMI controlled walk in the exoskeleton is 1100 ± 154.92 s (range: 892 to 1406 s); for comparison, a joystick control uses only 543 s which interestingly gains only a factor of two over brain control during task two (cf table 4). Note that joystick control is limited by the exoskeleton and that there may be a greater performance differential with a faster exoskeleton.

Figure 9(a) shows the canonical correlation variation which is calculated during the whole line tracing task when subject S1 walked in the exoskeleton. The horizontal lines indicate threshold values calculated from the offline experiment. The values which exceed the threshold are boldly lined.

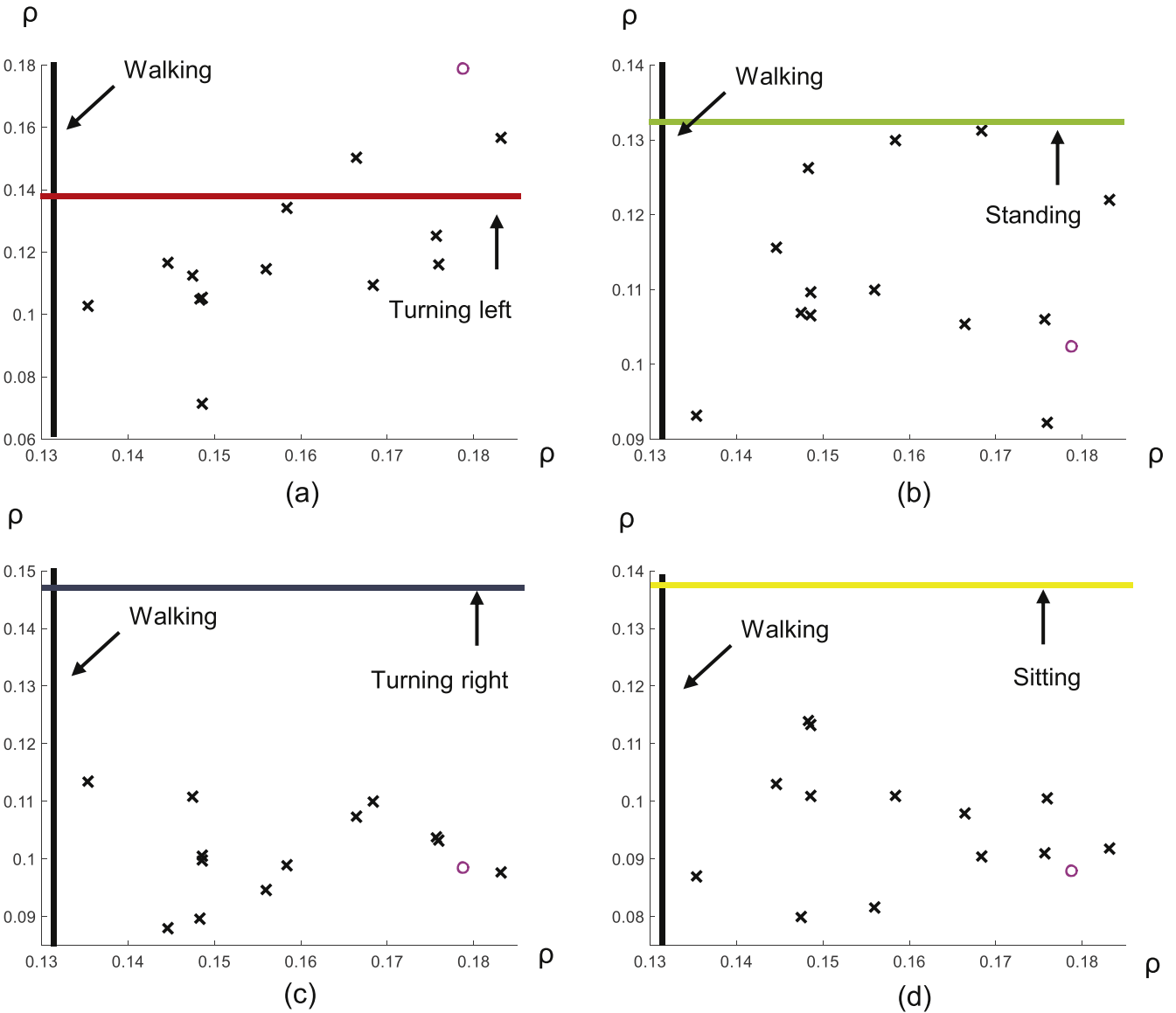


Figure 12. An example of the threshold classification method for S2; test data (purple diamond) with walking data is plotted on the ρ_1 axis with ρ_2 in (a), ρ_3 in (b), ρ_4 in (c), and ρ_5 in (d) respectively. A vertical line indicates the threshold of ρ_1 (walking). Horizontal lines indicate the threshold of ρ_2 (turning left) in (a), ρ_3 (standing) in (b), ρ_4 (turning right) in (c), and ρ_5 (sitting) in (d).

The correlation increases when the subject looks at the LED. Figure 9(b) presents the command changes. The exoskeleton's functions which are walking, turning right and turning left have an operation time of approximately 10 s. If the next commands are given 2 s before the movements finish, the exoskeleton moves continuously. Note that our system has an asynchronous control mode. Hence, if the canonical correlations do not exceed the threshold values, the system keeps the standing position. The subject S1 just needed 34 walking commands, seven right turn commands and six left turn commands to complete the line tracing task. Essentially, the exoskeleton walks in a straight line when walking forward. However, due to infinitesimal mechanical imbalances and optimal setting problems which are not precisely adjusted for each subject's body, fluctuations in the number of left and right commands exist.

3.3. Evaluation of classifier

In this section, we evaluate the degree of confusion between the different classifiers. The confusion matrix of offline data classification results by maximum value is given in figure 10(a), by threshold in (b), and by KNN is given in (c). The confusion matrix of online data classification results by maximum value is given in (d), by threshold is given in (e), and by KNN is given in (f). Fivefold cross-validation was used for the threshold and KNN method. We computed the accuracies using online experiment task one data with labels given from auditory cues and the predicted classes from each classifier. In the maximum-based classifier, more errors which are incorrectly labeled as left turns were predicted than others. We surmise that more 11 Hz errors come from potential changes in mu band, due to frequent eye closing or blinking [51]. However, these errors are reduced in the threshold

method and KNN. Most subjects showed basically higher SSVEP responses at 11 Hz than for other frequencies. Hence, misclassification as a left turn happened frequently for the maximum method.

Comparing the threshold method and KNN for online data, KNN showed a slightly higher accuracy. However, the threshold method can detect ambiguous features as rest states. We also provide the individual results of threshold and KNN (when $k = 5$) of offline and online data using fivefold cross-validation in tables 5 and 6. KNN recorded higher average accuracy in both sets of data.

The KNN results using fivefold cross-validation where $k = 1, 3, 5, 7$ are presented in table 7. The best accuracy was achieved for $k = 5$ in both data sets. In particular, S2 showed the biggest improved accuracy in KNN. An example of KNN for S2 is presented in figure 11. The test data point (purple diamond) is shown with all data plotted on the ρ_1 , ρ_2 , and ρ_3 axis. Furthermore, the distance of the K th nearest neighbor and the test data labels (when $k = 5$) are presented. According to the number of k labels, the test data was classified correctly for walking states.

However, there was a misclassification in the case of the threshold method. The reason is represented in figure 12. The same data is plotted on the ρ_1 axis with ρ_2 in (a), ρ_3 in (b), ρ_4 in (c), and ρ_5 in (d). The vertical and horizontal line indicate the threshold of each ρ_i . In figure 12(a), the correlation of the test data exceeded a threshold of ρ_1 as well as ρ_2 . The test data was thus erroneously classified as a left turn.

4. Conclusion

BMI control of exoskeletons can be a hard task due to artifacts in the EEG signal caused by ambulatory environments (see figure 5). These artifacts can be pronounced for some subjects and may be the result of multiple causes including suboptimal EEG measurements or broadband distortions due to the exoskeleton. For example, while walking in the exoskeleton a subject's head may be moved which can give rise to swinging movements in the line between electrodes and EEG amplifiers leading to disconnections or high impedance measurements in extreme cases. Such artifacts could be decreased by future improvements in mobile BMI technology and more robust signal processing [52]. With the current state of EEG and exoskeleton technology we have provided a simple yet highly effective and innovative contribution, namely to use the highly robust SSVEP paradigm which, due to its oscillatory nature, can demodulate a subject's intention comparatively easily and effectively despite signal-to-noise ratios which can be very unfavourable.

In our system, we used low frequency bands (from 9 to 17 Hz) since they yield large SSVEP responses and high performance despite exoskeleton induced artifacts. However, SSVEP in a lower frequency range may induce user fatigue during extended usage and may also carry a potential seizure risk. This may be resolved by using higher frequencies, however, due to smaller SSVEP responses at a slight reduction of system performance.

This paper has reported a successful online implementation of a lower limb exoskeleton control system based on an asynchronous SSVEP-BMI. Clearly, all 11 subjects acquired intuitive purposeful online BMI control of the exoskeleton immediately after a short offline experiment; in fact BMI control was attained following a training data collection procedure of only 8 min. While we have used a very simple five class CCA-based SSVEP classifier using a threshold value, KNN can improve further. However, we surmise that more sophisticated classification methods may still improve the presented results. From the perspective of man-machine interaction, the visual stimulation unit for the control interface is designed to enable intuitive control, and clearly all subjects would instantly be able to comprehend how to control the system.

In conclusion, our study provides striking evidence that SSVEP-based asynchronous BMI control of gait assistance robots in real life has become possible, despite the significant artifacts in EEG caused by the exoskeleton. The advantages of the proposed asynchronous BMI system is that many people can use SSVEPs very easily and with high accuracy [53] as it only requires ocular movements and attention to visual stimuli. Furthermore our BMI system offers a short training time.

Future work will target the evaluation of system performance with end user groups and also investigate possible use in the context of gait rehabilitation. Special attention will be given to research on decreasing visual fatigue from SSVEP stimuli and the exploration of the limits for patients unable to fixate.

Acknowledgments

This research was supported by a National Research Foundation of Korea (NRF) grant funded by the Korea government (NRF-2015R1A2A1A05001867).

References

- [1] Lebedev M A and Nicolelis M A L 2006 Brain-machine interfaces: past, present and future *Trends Neurosci.* **29** 536–46
- [2] Dornhege G, Millan J, Hinterberger T, McFarland D and Müller K-R (ed) 2007 *Toward Brain Computer Interfacing* (Cambridge, MA: MIT Press)
- [3] Hochberg L R et al 2006 Neuronal ensemble control of prosthetic devices by a human with tetraplegia *Nature* **442** 164–71
- [4] Collinger J L et al 2013 High-performance neuroprosthetic control by an individual with tetraplegia *The Lancet* **381** 557–64
- [5] Lopes A C, Pires G and Nunes U 2013 Assisted navigation for a brain-actuated intelligent wheelchair *Robot. Auton. Syst.* **61** 245–58
- [6] Carlson T and del Millán J R 2013 Brain-controlled wheelchairs: a robotic architecture *IEEE Robot. Autom. Mag.* **20** 65–73

- [7] Pfurtscheller G, Müller G R, Pfurtscheller J, Gerner H J and Rupp R 2003 Thought-control of functional electrical stimulation to restore hand grasp in a patient with tetraplegia *Neurosci. Lett.* **351** 33–36
- [8] Schultz A and Kuiken T 2011 Neural interfaces for control of upper limb prostheses: the state of the art and future possibilities *PM R* **3** 55–67
- [9] Pfurtscheller G and Neuper C 2001 Motor imagery and direct brain-computer communication *Proc. IEEE* **89** 1123–34
- [10] Gao S, Wang Y, Gao X and Hong B 2014 Visual and auditory brain-computer interfaces *IEEE Trans. Biomed. Eng.* **61** 1436–47
- [11] Yeom S-K, Fazli S, Müller K-R and Lee S-W 2014 An efficient ERP-based brain-computer interface using random set presentation and face familiarity *PLoS One* **9** e111157
- [12] Blankertz B, Tomioka R, Lemm S, Kawanabe M and Müller K-R 2008 Optimizing spatial filters for robust EEG single-trial analysis *IEEE Signal Process. Mag.* **25** 41–56
- [13] Blankertz B, Lemm S, Treder M, Haufe S and Müller K-R 2011 Single-trial analysis and classification of ERP components tutorial *NeuroImage* **56** 814–25
- [14] Lotte F, Congedo M, Lécuyer A, Lamarche F and Arnaldi B 2007 A review of classification algorithms for EEG-based brain-computer interfaces *J. Neural Eng.* **4** 1–13
- [15] Lemm S, Blankertz B, Dickhaus T and Müller K-R 2011 Introduction to machine learning for brain imaging *Neuroimage* **56** 387–99
- [16] Lotte F and Guan C 2012 Regularizing common spatial patterns to improve BCI designs: unified theory and new algorithms *IEEE Trans. Biomed. Eng.* **58** 355–62
- [17] Suk H-I and Lee S-W 2013 A novel bayesian framework for discriminative feature extraction in brain-computer interfaces *IEEE Trans. Pattern Anal. Mach. Intell.* **35** 286–99
- [18] Tomioka R and Müller K-R 2010 A regularized discriminative framework for EEG analysis with application to brain-computer interface *Neuroimage* **49** 415–32
- [19] Blankertz B et al 2010 Neurophysiological predictor of SMR-based BCI performance *Neuroimage* **51** 1303–9
- [20] Gramann K, Gwin J T, Bigdely-Shamlo N, Ferris D P and Makeig S 2010 Visual evoked responses during standing and walking *Front. Hum. Neurosci.* **4** 202
- [21] Müller-Putz G R and Pfurtscheller G 2008 Control of an electrical prosthesis with an SSVEP-based BCI *IEEE Trans. Biomed. Eng.* **55** 361–4
- [22] Ortner R, Allison B Z, Korisek G, Guggl H and Pfurtscheller G 2011 An SSVEP BCI to control a hand orthosis for persons with tetraplegia *IEEE Trans. Neural. Syst. Rehabil. Eng.* **19** 1–5
- [23] Zhu D, Bieger J, Garcia Molina G and Aarts R M 2010 A survey of stimulation methods used in SSVEP-based BCIs *Comput. Intell. Neurosci.* **2010** 702357
- [24] Parini S, Maggi L, Turconi A C and Andreoni G 2009 A robust and self-paced BCI system based on a four class SSVEP paradigm: algorithms and protocols for a high-transfer-rate direct brain communication *Comput. Intell. Neurosci.* **2009** article 864564
- [25] Luo A and Sullivan T J 2010 A user-friendly SSVEP-based brain-computer interface using a time-domain classifier *J. Neural Eng.* **7** 26010–9
- [26] Zhang Y, Jin J, Qing X, Wang B and Wang X 2012 LASSO based stimulus frequency recognition model for SSVEP BCIs *Biomed. Signal Process. Control* **7** 104–11
- [27] Lin Z, Zhang C, Wu W and Gao X 2007 Frequency recognition based on canonical correlation analysis for SSVEP-based BCIs *IEEE Trans. Biomed. Eng.* **54** 2610–4
- [28] McDaid A J and Xie S Q 2013 Brain controlled robotic exoskeleton for neurorehabilitation *Proc. of the IEEE/ASME Int. Conf. on Advanced Intelligent Mechatronics (Wollongong, Australia)* pp 1039–44
- [29] Diez P F, Mut V A, Perona E M A and Leber E L 2011 Asynchronous BCI control using high-frequency SSVEP *J. Neuroeng. Rehabil.* **8** 39–46
- [30] Lin Y-P, Wang Y and Jung T-P 2013 A Mobile SSVEP-based brain-computer interface for freely moving humans: the robustness of canonical correlation analysis to motion artifacts *Proc. of the XXXV IEEE Ann. Int. Conf. of the EMBS (Osaka, Japan)* pp 1350–3
- [31] Kim I-H, Kim J-W, Haufe S and Lee S-W 2015 Detection of braking intention in diverse situations during simulated driving based on EEG feature combination *J. Neural Eng.* **12** 016001
- [32] Müller K-R et al 2008 Machine learning for real-time single-trial analysis: from brain–computer interfacing mental state monitoring *J. Neurosci. Methods* **167** 82–90
- [33] King C E, Wang P T, Chui L A, Do A H and Nenadic Z 2013 Operation of a brain–computer interface walking simulator for individuals with spinal cord injury *J. Neuroeng. Rehabil.* **10** 77–90
- [34] Do A H, Wang P T, King C E, Chun S N and Nenadic Z 2013 Brain-computer interface controlled robotic gait orthosis *J. Neuroeng. Rehabil.* **10** 111–9
- [35] Kilicarslan A, Prasad S, Grossman R G and Contreras-Vidal J L 2013 High accuracy decoding of user intentions using EEG to control lower-body exoskeleton *Proc. of the XXXV IEEE Ann. Int. Conf. of the EMBS (Osaka, Japan)* pp 5606–9
- [36] Contreras-Vidal J L and Grossman R G 2013 NeuroRex: a clinical neural interface roadmap for eeg-based brain machine interfaces to a lower body robotic exoskeleton *Proc. of the XXXV IEEE Ann. Int. Conf. of the EMBS (Osaka, Japan)* pp 1579–82
- [37] Venkatakrishnan A, Francisco G E and Contreras-Vidal J L 2014 Applications of brain-machine interface systems in stroke recovery and rehabilitation *Curr. Phys. Med. Rehabil. Rep.* **2** 93–105
- [38] Nilsson A, Vreeke K S, Haglund V, Kawamoto H, Sankai Y and Borg J 2014 Gait training early after stroke with a new exoskeleton—the hybrid assistive limb: a study of safety and feasibility *J. Neuroeng. Rehabil.* **11** Article 92
- [39] Tsukahara A, Hasegawa Y, Eguchi K and Sankai Y 2015 Restoration of gait for spinal cord injury patients using hal with intention estimator for preferable swing speed *IEEE Trans. Neural. Syst. Rehabil. Eng.* **23** 308–18
- [40] Rea M et al 2014 Lower limb movement preparation in chronic stroke: a pilot study toward an FNIRS-BCI for gait rehabilitation *Neurorehabil. Neural Repair* **28** 564–75
- [41] Crus-Garza J G, Hernandez Z R, Nepaul S, Bradley K K and Contreras-Vidal J L 2014 Neural decoding of expressive human movement from scalp electroencephalography (EEG) *Front. Hum. Neurosci.* **8** 188
- [42] Contreras-Vidal J L 2014 Identifying engineering, clinical and patient's metrics for evaluating and quantifying performance of brain-machine interface (BMI) system *Proc. of the IEEE Int. Conf. on Systems Man, and Cybernetics (San Diego, USA)* pp 489–92
- [43] Tucker M et al 2015 Control strategies for active lower extremity prosthetics and orthotics: a review *J. Neuroeng. Rehabil.* **12** 1
- [44] Kwak N-S, Müller K-R and Lee S-W 2014 Toward exoskeleton control based on steady state visual evoked potentials *Proc. of the IEEE International Winter Workshop on Brain-Computer Interface (Gangwon, Korea)* pp 33–34
- [45] Pastor M A, Artieda J, Arbizu J, Valencia M and Masdeu J C 2003 Human cerebral activation during steady-state visual-evoked responses *J. Neurosci.* **23** 11621–7 14684864
- [46] Biesmann F, Plis S, Meinecke F C, Eichele T and Müller K-R 2011 Analysis of multimodal neuroimaging data *IEEE Rev. Biomed. Eng.* **4** 26–58

- [47] Fazli S, Dähne S, Samek W, Biessmann F and Müller K-R 2015 Learning from more than one data source: data fusion techniques for sensorimotor rhythm-based brain–computer interfaces *Proc. IEEE* **103** 891–906
- [48] Picton T W, John M S, Dimitrijevic A and Purcell D 2003 The human auditory steady-state evoked potentials *Int. J. Audiol.* **42** 177–219
- [49] Dähne S, Meinecke F C, Haufe S, Höhne J, Tangermann M, Müller K-R and Nikulin V V 2014 SPoC: a novel framework for relating the amplitude of neuronal oscillations to behaviorally relevant parameters *NeuroImage* **86** 111–22
- [50] Wolpaw J R, Ramoser H, McFarland D J and Pfurtscheller G 1998 EEG-based communication: improved accuracy by response verification *IEEE Trans. Rehabil. Eng.* **6** 326–33
- [51] Barry R J, Clarke A R, Johnstone S J, Magee C A and Rushby J A 2007 EEG differences between eye-closed and eyes-open resting conditions *Clin. Neurophysiol.* **118** 2763–73
- [52] Samek W, Kawanabe M and Müller K-R 2014 Divergence-based framework for common spatial patterns algorithms *IEEE Reviews in Biomedical Engineering* **7** 50–72
- [53] Guger C et al 2012 How many people could use an SSVEP BCI? *Front. Neurosci.* **6** 169 Article